Influence of Sulfur Incorporation into Nanoporous Anodic Alumina on the Volume Expansion and Self-Ordering Degree

Rodríguez-López, S.; Mínguez-Bacho, Ignacio; Climent, A.; Fichou, Denis; Vázquez, M.; Hernández-Vélez, M.

2015

Mínguez-Bacho, I., Rodríguez-López, S., Climent, A., Fichou, D., Vázquez, M., & Hernández-Vélez, M. (2015). Influence of Sulfur Incorporation into Nanoporous Anodic Alumina on the Volume Expansion and Self-Ordering Degree. The Journal of Physical Chemistry C, 119(49), 27392-27400.

https://hdl.handle.net/10356/81723

https://doi.org/10.1021/acs.jpcc.5b06928

THE JOURNAL OF PHYSICAL CHEMISTRY C

Article

pubs.acs.org/JPCC

Influence of Sulfur Incorporation into Nanoporous Anodic Alumina on the Volume Expansion and Self-Ordering Degree

I. Mínguez-Bacho,[†,‡,○] S. Rodríguez-López,[§,∥,□] A. Climent,[§,⊥] D. Fichou,[*,‡,@,▽] M. Vázquez,[†] and M. Hernández-Vélez[*,†,§]

[†]Instituto de Ciencia de Materiales de Madrid, Consejo Superior de Investigaciones Científicas, Cantoblanco, 28049 Madrid, Spain
[‡]School of Physical and Mathematical Science, Nanyang Technological University, 637371 Singapore
[§]Departamento de Física Aplicada, Universidad Autónoma de Madrid (UAM), Cantoblanco, ES-28049 Madrid, Spain
[∥]Instituto de cerámica y vidrio, Consejo Superior de Investigaciones Científicas, Cantoblanco, 28049 Madrid, Spain
[⊥]Centro de Micro-Análisis de Materiales (CMAM), Cantoblanco, 28049 Madrid, Spain
[@]Sorbonne Universités, UPMC Univ Paris 06, UMR 8232, Institut Parisien de Chimie Moléculaire, F-75005 Paris, France
[▽]CNRS, UMR 8232, Institut Parisien de Chimie Moléculaire, F-75005 Paris, France

Supporting Information

ABSTRACT: Self-ordering degree of anodic alumina nanopores is related to the volume expansion of the aluminum oxide. However, little is known about how the ionic species derived from electrolyte affect parameters inducing self-ordering of the nanopores. The influence of sulfur incorporation into nanoporous anodic aluminum oxide (AAO) films on volume expansion and self-ordering degree has been investigated under potentiostatic conditions (14−25 V) in different sulfuric acid electrolytes (3−20 wt %), the average current densities of each anodization being in the range of 0.1−10 mA cm^{-2}. Rutherford backscattering spectroscopy (RBS) reveals that the incorporation of sulfur species into AAO, as well as the volume expansion factor (VEF), follows a logarithmic dependence on the average current density regardless of the applied voltage and sulfuric acid concentration. The relationship between volume expansion and the S/Al ratio is linear for each concentration of acid in the electrolyte. Furthermore, self-ordering regimes are also revealed for each acid concentration at VEF in the range of 1.50−1.66. We suggest that plasticity, enhanced by sulfur incorporation, counterbalances the high mechanical stress generated by volume expansion, thus inducing new self-ordering regimes. These new regimes are dependent not only on VEF but also on a subtle equilibrium between stress and plasticity of the nanoporous AAO films.

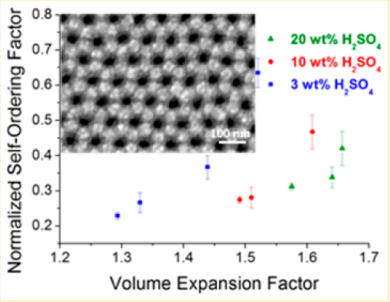

1. INTRODUCTION

Nanostructured metal oxides are abundant and low-cost materials that find applications in various field such as electronics, catalysis, batteries, supercapacitors, and solar energy conversion.[1−3] The most common materials used for these applications are based on transition metal oxides.[4−6] Anodization is a cost-efficient method to grow nanostructures based on these materials for energy applications.[7−9] Recent studies on the formation of nanostructured anodic aluminum oxide (AAO) films underpin the importance, variety, and complexity of the growth mechanism when a wide range of experimental conditions are available.[10] Nanostructured AAO films are being applied in multiple fields as biosensors,[11,12] optical sensors,[13,14] magneto-thermoelectric and magneto-caloric materials,[15,16] and the study of magnetic properties of nanowires.[17−19] Therefore, it is of utmost importance to develop new methods to design novel forms of nanostructured AAO films by controlling their growth mechanism.[20−22]

As-grown anodic alumina possesses an amorphous structure. Nanoporous AAO is composed by barrier layer, cylindrical nanochannels perpendicularly oriented to the surface and parallel among them with, ideally, an hexagonal arrangement.[23] Alumina formation takes place under different elementary reactions at the metal-oxide and oxide-electrolyte interfaces by ion migration (Al^{3+} outward and O^{2-} or OH^- inward) within the barrier layer.[24,25] Ion migration, together with the formation of pores, is governed by the electric field generated through the barrier layer.[26,27] Anion incorporation coming from different electrolytes into the alumina matrices has long been the focus of intense research.[28,29] More recently, the growth mechanisms of anodic alumina have been investigated by García-Vergara et al. in a series of publications.[30−32] It has been shown that anodization parameters such as current density, anodizing voltage, and temperature affect the quantity of incorporated anions coming from the electrolyte.[33−35] The incorporation of anionic species influences macroscopic properties such as

Received: July 17, 2015
Revised: November 3, 2015
Published: November 12, 2015

DOI: 10.1021/acs.jpcc.5b06928
J. Phys. Chem. C 2015, 119, 27392−27400

photoluminescence[36,37] or elasticity.[38] On the other hand, volume expansion during anodization plays a crucial role in the growth and morphology of nanoporous AAO films. Ideally, volume expansion can be quantified by the Pilling-Bedworth ratio (PBR). The PBR is the ratio between the volume of oxide and the volume of metal (here aluminum) from which the oxide is grown, taking into account the oxide density and its molecular weight. These values are difficult to determine precisely due to impurities incorporated into the nanoporous AAO films. Therefore, the volume expansion is determined by the ratio between the thickness of the nanoporous AAO film and the thickness of aluminum necessary for the film formation. In addition, some works have studied the evolution of the volume expansion factor regarding current density, anodization temperature, and electrolytic solutions.[39−44] Volume expansion of nanoporous AAO films has been studied as a determining factor for nanoporous self-ordering conditions.[45] The value of the volume expansion factor required for achieving self-ordered nanoporous has been reported to be between 1.2 and 1.4 independently on the acidic electrolyte.[46,47] Quantification of the self-ordering degree is a very important task in order to understand the formation mechanism of hexagonal ordered structures. The quantification of the self-ordering degree is possible by using tools to evaluate self-ordering of nanopores based on pair distribution and self-correlation functions.[48−53] Recently, several works have studied the formation of ordered nanopore arrays in anodic alumina.[54,55]

In this work, we have focused our attention to the influence of sulfuric acid solutions with different concentration (3−20 wt %) as electrolytes under different applied voltages (14−25 V) in the growth of nanoporous AAO films. Thus, we start reporting a detailed study of sulfur incorporation in the bulk alumina. We also have calculated the growth rate, volume expansion behavior, and formation efficiency in the fabrication of these porous materials under different experimental conditions. The results achieved about the control of several significant fabrication parameters will allow us to evaluate some features such as self-ordering arrangements, which are nowadays not discussed enough in the literature.

2. EXPERIMENTAL SECTION

Aluminum discs (99.999%, Goodfellow) of 2.5 cm diameter are degreased by sonicating during 5 min in acetone, ethanol, and diwater in sequential order. Right after, aluminum discs are electropolished in a 25% HClO4 and 75% EtOH mixture under 20 V of applied voltage, during 3 min at temperature around 10 °C and vigorous stirring. Aluminum discs are anodized by means of a two-step potentiostatic anodization process described elsewhere.[56] These processes are carried out in a homemade Teflon electrochemical cell. This cell is provided with a cooling chamber allowing continuous flow of cooling liquid at constant temperature of 0 °C in order to keep a uniform temperature during the anodization processes. The cathode is constituted by a net of platinum wire placed at 1 cm from the anode. This setup ensures a uniform electric field on the surface of the substrate. Aluminum discs are anodized in different sulfuric acid, H_2SO_4, electrolytes with concentrations of 3, 10, and 20 wt % (A, B, and C series, respectively). The applied anodization voltages are 25, 20, 17, and 14 V for each electrolyte during 16 h for the first anodization. Next, the resulting nanoporous AAO film is chemically removed as described elsewhere.[57] The second anodization is carried out during 150 min for A series and 20 min for B and C series. The same constant stirring rate is applied during all the anodization processes. These experimental parameters and sample labels are summarized in Table 1. The current densities are registered for each sample. The top surfaces of the different samples are analyzed by high-resolution scanning electron microscopy (Philips XL-30, FEG-HRSEM).

Table 1. Sample Labels as a Function of Acid Concentration of the Electrolyte and Applied Voltages during the Anodization Process

		applied voltages (V)			
sample series	$[H_2SO_4]$ (wt %)	25	20	17	14
A	3	A25	A20	A17	A14
B	10	B25	B20	B17	B14
C	20	C25	C20	C17	C14

Rutherford backscattering spectrometry (RBS) experiments were carried out in the 5 MV tandem accelerator at the Microanalysis Centre of Materials (CMAM).[58] Helium ions, He^+, at 3035 eV are used to receive the RBS spectra (oxygen resonance conditions). The spectra are simulated with SIMNRA.[59]

3. RESULTS AND DISCUSSION

3.1. Current Density Analysis. The evolution of the current densities for each given anodization voltage reaches a steady state. The steady state is associated with homogeneous growth in mild anodization conditions.[60] However, the current densities evolution for samples B25 and C25 are nonuniform and very high. These behaviors of the current densities leads to an effect called "white burning",[61] which induces mechanical instabilities in the nanoporous AAO films. The average current densities (j_{AVG}) registered for the A, B, and C series have been plotted in Figure S1. The average current densities for each anodization process are always below 10 mA/cm^2. The typical exponential dependende of the current density under high-field conditions on the applied voltage can be observed (Figure S1).[62] This behavior is associated with the transfer of ions and the potential drop through the barrier layer following the equation associated with high-field conduction theory,[26] $j = j_0 \exp(\beta\Delta U/d_{BL})$, where j_0 and β are constants which depend on the material, j represents current density, ΔU is the anodizing voltage, and d_{BL} is the thickness of the barrier layer. At the same time, the average current densities increase for each electrolyte concentration (3, 10, and 20 wt %) at a given applied voltage.

3.2. RBS Analysis. The signals of sulfur, oxygen, and aluminum elements are identified in all spectra. Wide spectrum from sample A25 is shown in Figure 1a. The edges found at 1840, 1700, and 1100 eV correspond to sulfur, aluminum, and oxygen elements, respectively.

A magnification of the RBS signal on the region of the S edge shows the detected quantity for samples anodized at 25 V in electrolytes with sulfuric acid concentration of 3, 10, and 20 wt % (Figure 1b). The same magnification of RBS signal for samples anodized at 20, 17, and 14 V, respectively, are presented in Figure S2. For each given anodization voltage (25, 20, 17, or 14 V), the concentration of sulfur atoms embedded into the nanoporous AAO film increase with the concentration of sulfuric acid used in the anodization process (3, 10, and 20 wt % H_2SO_4). On the other hand, there are no significant variations on the concentration of Al and O nuclei detected. If the sulfur signals are compared among them as a function of the

DOI: 10.1021/acs.jpcc.5b06928
J. Phys. Chem. C 2015, 119, 27392−27400

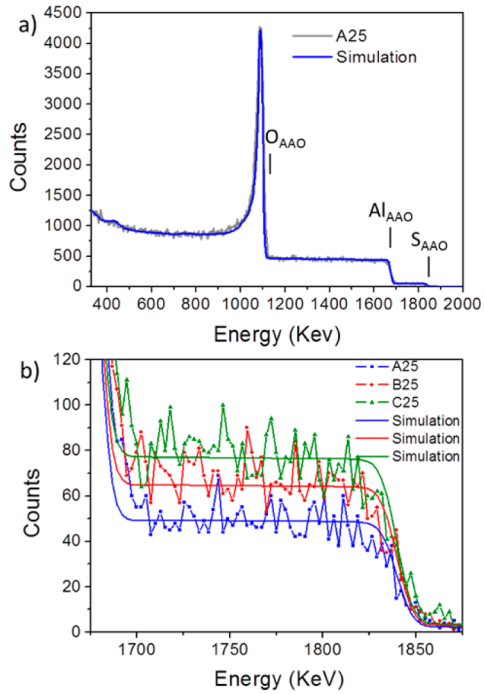

Figure 1. Rutherford backscattering spectroscopy (RBS) spectra for (a) nanoporous AAO from sample A25 and its simulated signal (blue line). The signals from sulfur, aluminum, and oxygen arising from the nanoporous AAO film are indicated as S_{AAO}, Al_{AAO}, and O_{AAO}, respectively. (b) Close-up representation in the 1700−1850 keV energy range of the RBS spectra of S nuclei embedded in the nanoporous AAO films from the A, B, and C sample series (blue, red, and green, respectively) and their corresponding simulated spectra (plain lines). The nanoporous AAO films are grown under anodization voltages of 25 V.

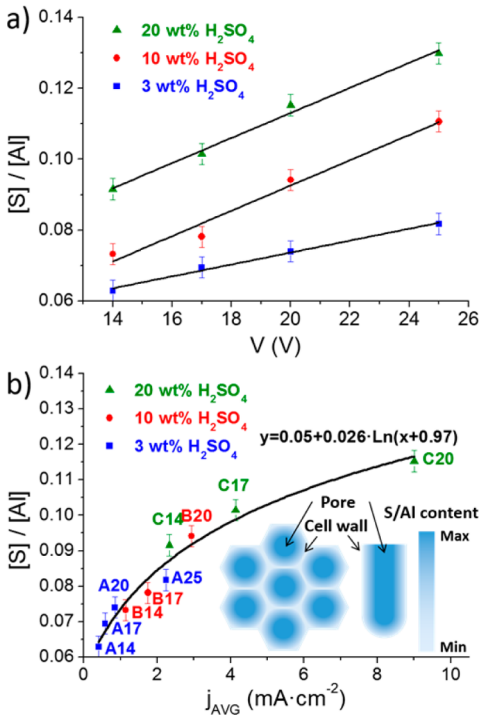

Figure 2. Ratio of normalized sulfur and aluminum concentrations embedded into the nanoporous AAO films for 3 (blue), 10 (red), and 20 (green) wt % H_2SO_4 and their dependence upon (a) the applied voltage and (b) the average current density (inset: scheme of top view and cross section of S/Al content and distribution in the alumina cells).

applied voltages (i.e., for a given electrolyte concentration used during anodization) then the quantity of nuclei detected decreases together with the anodization voltage. It is well-known that the anionic species coming from the electrolyte are not homogeneously incorporated to the alumina matrix.[26,63] Patermarakis et al. also showed a bell-like distribution of anionic impurities in the barrier layer, wall cell, and along the thickness of the film.[64,65] The RBS spectra shown in Figure 1b is possible to observe an abrupt increase of the sulfur nuclei as an energy decrease from 1850 to 1825 keV, which is attributed to the ions backscattered on the very surface of the sample. In addition, a slight increase of sulfur nuclei concentration could be possible to interpret as an energy decrease from 1825 to 1775 keV. In this range of energies, we also have to take into account the roughness of the surface with the ridges of the pores on the surface. However, the scope of the RBS analysis of this work is to calculate an average quantity of sulfur nuclei concentration for each sample. Therefore, we can assume a uniform distribution of sulfur nuclei throughout the thickness of the sample for the simulation of the RBS spectra.

The ratio between normalized concentration of sulfur and aluminum embedded in the nanoporous AAO films and its dependence on the applied voltage and average current densities of the anodization processes is shown in Figure 2. The ratio [S]/[Al] has a linear dependence on the applied voltage during the anodization Figure 2a. The incorporation of sulfur to nanoporous AAO films regarding aluminum content increases linearly with the applied voltage. The linear dependence of anion incorporation with the applied voltage is also confirmed for oxalic electrolytes in other works.[66] It is also observed that the ratio [S]/[Al] increases as a function of sulfuric acid concentration of the electrolyte. These results can be explained by the increase of current density, and it is related to the high-field conduction theory. The ratio [S]/[Al] has a linear dependence with the voltage, hence also with the electric field. Therefore, following the equation of high-field conduction theory, the current density would have an exponential dependence on the [S]/[Al] ratio. However, from the thermodynamical point of view, the incorporation of sulfur into the nanoporous AAO film is a consequence of the current density (i.e., actually the [S]/[Al] ratio depends on the current density). In Figure 2b, the [S]/[Al] ratio is presented as a function of the current density. The evolution of the [S]/[Al] ratio with the current density shows a dependence which is proportional to the logarithm of the current density and satisfies the general relation $y = a + b \times \ln(x + c)$, where in this case, y is [S]/[Al], x is current density (j), a and b are material dependent constants, and c is a constant current density (j_0). From the fitting of the curve, it is possible to say that the sulfur incorporation regarding aluminum atoms in the alumina follows this equation: $[S]/[Al] = 0.05 + 0.026 \times \ln(j + 0.97)$. The anion incorporation derived from the electrolyte (in this case, SO_4^-), as well as oxygen containing anions (O^{2-} and OH^-), moves inward through the electrolyte/oxide and oxide/metal interface. This anion migration is governed by the electric field generated at the barrier layer of the nanoporous AAO.[67]

The above result agrees with other studies where the incorporation of SO_4^{-2} anions occur mainly in the linked form.[29] This incorporation has its origin in the barrier layer

DOI: 10.1021/acs.jpcc.5b06928
J. Phys. Chem. C 2015, 119, 27392−27400

conversion to the porous alumina formation. During the steady state growth, the anionic species derived from the electrolyte are incorporated to the outer layer of the alumina matrix at the electrolyte/oxide interface, as shown in the inset of Figure 2b. Stępniowsky et al. also observed that the mentioned areas of alumina depend on the region and the interface where different reactions take place during the formation of alumina allowing the incorporation of sulfate ions.[68]

3.3. Growth Rates. Growth rates of nanoporous AAO films are calculated by direct measurement of the thickness of each film from SEM cross sectional view images (Table S1) and dividing by a second anodization time. The growth process for samples B25 and C25 is not uniform, so it is not possible to establish the growth rates for them. Growth rates are presented as a function of the applied voltage during the anodization and their respective average current densities (Figure S3).

The growth rates of nanoporous AAO increase together with the electrolyte concentration and applied voltages. More specifically, there is an exponential dependence of the growth rate with the applied voltage (Figure S3a). On the other hand, a linear dependence of the growth rates on the average current densities of each sample is observed (Figure S3b). The same exponential dependence on the applied voltage is observed for the growth rates (Figure S3a) and the average current densities (Figure S1). Therefore, there must be a linear dependence between the growth rates and the average current densities as shown in Figure S3b. Consequently, the incorporation of sulfate ions to nanoporous AAO films has exactly the same dependence on the growth rate than on the average current density as shown in Figure 2b. The slopes of the linear fit of the three segments correspond to the three different electrolyte concentrations (Figure S3b). The increase of the slope for each segment belonging to each electrolyte concentration implies a higher alumina yield during the anodization processes. Hence, it would be possible to infer that there is an increasing tendency on the volume expansion factor of the nanoporous AAO films and efficiency on the anodization process.

3.4. Volume Expansion Factor. The volume expansion factor is evaluated as the ratio between the thickness of the nanoporous AAO film generated from the anodized aluminum atoms and the thickness of consumed aluminum film during the process. In order to calculate the thickness of consumed Al during the anodization process we use the Faraday's Law for electrolysis in terms of thickness (eq 1).

$$\frac{\sigma}{F} \times \frac{\mathrm{At}_{W_{Al}}}{z} = \rho_{Al} h \tag{1}$$

where σ is the charge density, F is the Faraday's constant, $\mathrm{At}_{W_{Al}}$ is the atomic weight of aluminum, z is the valence number, ρ_{Al} is the aluminum density, and h is the thickness of consumed aluminum. It can be assumed that on the aluminum electrode only aluminum ions (Al^{3+}) are generated during the anodization process. The values of the charge density and thickness of consumed aluminum and nanoporous AAO films are presented in Table S1. Volume expansion factor values obtained from the calculations are presented in Figure 3.

The volume expansion factor of the prepared nanoporous AAO films range from 1.29 up to 1.66. The volume expansion factor has a linear dependence with the applied voltage (Figure 3a). This behavior is supported by other results obtained in sulfuric and oxalic acid by Vrublevsky et al.[39,40] Figure 3a also shows that the volume expansion factor increases with the

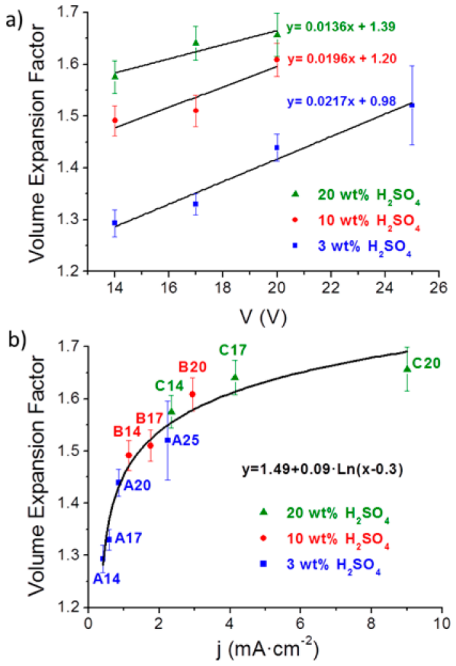

Figure 3. Volume expansion factor of nanoporous AAO films grown in 3 (blue), 10 (red), and 20 (green) wt % H_2SO_4 for the A, B, and C sample series, respectively. The volume expansion factor is represented as a function of (a) the applied voltage and (b) the average current density.

sulfuric acid electrolyte concentration (3, 10, and 20 wt %). The linear increase of the volume expansion factor is common to all the electrolyte concentrations, and the slope values of the linear fits decrease as the electrolyte concentration increases (Table 2). In order to have a general view of the volume expansion factor in sulfuric acid based electrolytes, our results are compared with other values obtained in different works under both potentiostatic and galvanostatic conditions (Table 2).

It is well-known that the temperature of the anodization process is a key factor to achieve self-ordering conditions.[69−72] However, we have observed that temperature has a slight effect on the volume expansion of alumina independently whether the process is in self-ordering conditions or not. This observation is based on the comparison of our results and the results presented in other works mentioned right after. The slight effect of temperature in the volume expansion factor has been observed for different temperature variations in sulfuric acid based electrolytes (ΔT = 20 °C)[41,43] and negligible effects for small variations (ΔT = 4 °C) for sulfuric and oxalic-based electrolytes.[39,40] Particularly, our results in the B series (10 wt % H_2SO_4) ($y = 0.0196x + 1.2$ at 0 °C) are in good agreement with those obtained for similar experimental conditions but anodization temperature ($y = 0.017x + 1.15$ at room temperature).[44] These two facts are compatible since volume expansion of alumina is not a key factor to achieve self-ordering conditions. This is because volume expansion is a consequence of other parameters like voltage, current density, electrolyte, or temperature. On the other hand, we have compared our results obtained in potentiostatic conditions to others in galvanostatic conditions.[39,41] We find that the relation between the volume expansion factor and the applied voltage are quite similar and the differences can be attributed to different anodization temperatures (ΔT = 20 °C) and different current density

DOI: 10.1021/acs.jpcc.5b06928
J. Phys. Chem. C 2015, 119, 27392−27400

Table 2. Volume Expansion Factor (VEF) of Nanoporous AAO Grown in Electrolytes Containing Various H_2SO_4 Concentrations under Different Experimental Conditions such as Temperature (T), Applied Voltage (V), and Current Density (j)[a]

[H_2SO_4]	T (°C)	V (V)	j (mA cm^{-2})	VEF [vs V (V)]	ref
20 wt %	0	14−20*	2.33−9.00	0.0136V + 1.39	this work
10 wt %	0	14−20*	1.14−2.93	0.0196V + 1.20	this work
3 wt %	0	14−25*	0.41−2.24	0.0217V + 0.98	this work
1 M (9.4 wt %)	RT	5−22*	NA	0.017V + 1.15	44
10 wt %	18−22	13−25	6−20*	0.0217V + 1.1	39
2.55 mol dm^{-3} (22.45 wt %)	0	17−40.8	5−50*	1.58−1.88	41
2.55 mol dm^{-3} (22.45 wt %)	20	8.1−29.7	5−50*	1.45−1.66	41
20 wt %	1	18−25*	NA	0.86−1.62	47
20 wt %	1	19*	NA	1.41	46
1.7 wt %	1	25*	NA	1.36	46
1.7 wt %	10	25*	NA	1.40	46

[a]Our results (see the three first lines of this table) are compared with values found in literature.

ranges of study. This similar behavior between galvanostatic and potentiostatic anodization conditions is due to the fact that during potentiostatic conditions, the current density reaches a steady-state (i.e., the current density is very stable). Consequently, anodization conditions under potentiostatic steady-state growth can be comparable to those of galvanostatic anodization. The volume expansion factor is also represented as a function of the average current density (Figure 3b). We could differentiate two regions in the evolution of volume expansion factor: one region of abrupt increase for low average current densities (0−5 mA cm^{-2}) and another region of linear increase for intermedium average current densities (>5 mA cm^{-2}). Figure 3b importantly shows that the tendency of the volume expansion factor is nearly independent of the concentration of the electrolyte. Therefore, for a given anodization temperature, the volume expansion factor of nanoporous AAO films on sulfuric acid based electrolytes strongly depends on the current density (Figure 3b). While Zhou et al.[41] show a study in the range of current densities under galvanostatic conditions from 5 to 50 mA cm^{-2}, our work focuses on lower average current densities from 0 to 10 mA cm^{-2}, both at 0 °C. These two works overlap and show clearly the two different trends for high and low current densities. The evolution of the volume expansion factor with the current density is proportional to the logarithm of the current density (i.e., inversely); the current density is proportional to an increasing exponential function of the volume expansion factor. Figure 3a shows that the volume expansion factor is linearly proportional to the voltage, which means that the volume expansion would be related to the electric field.[73] Therefore, an increase of the electric field would imply an increase of the volume expansion factor.[40] The increase of the sulfuric acid concentration in the electrolyte increases the field-assisted flow at the barrier layer for a given voltage. Therefore, the barrier layer thickness decreases, which implies that the current density increases. As we have already mentioned, the high-field conduction theory shows that the current density has an exponential dependence on the electric field. In consequence, the electric field at the barrier layer also increases with the average current density. This behavior is confirmed by the logarithmic dependence of the volume expansion factor with the current density (Figure 3b).

Figure 4 represents the evolution of the volume expansion factor with the sulfur incorporation from the electrolyte to the nanoporous AAO films. It is worth noting that the values of volume expansion and sulfur incorporation are values

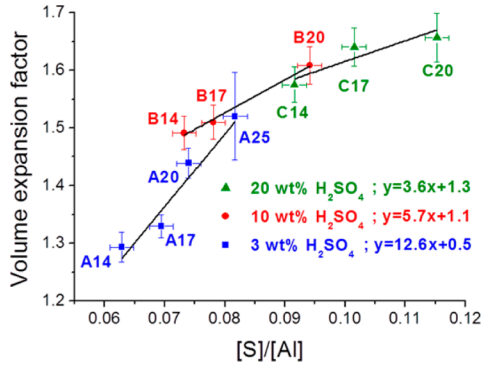

Figure 4. Volume expansion factor of nanoporous AAO films as a function of the S/Al ratio. Nanoporous AAO films are grown in 3 (blue), 10 (red), and 20 (green) wt % H_2SO_4 (A, B, and C series, respectively).

consequent of the applied experimental conditions. Therefore, volume expansion is not only a function of the S/Al ratio and vice versa. The ratio [S]/[Al] increases linearly with the volume expansion factor for each sulfuric acid concentration of the electrolyte. Figure 4 shows slopes of 3.6, 5.7, and 12.6 for 3, 10, and 20 wt % concentration of sulfuric acid in the electrolyte. From the trend of the slopes, we can infer that the volume expansion is self-limited independently on the increase of sulfur incorporation in the nanoporous AAO. The linear increase of the volume expansion factor with the sulfur incorporation was expected since both of them have similar linear dependence on the applied voltage (Figure 2a and Figure 3a) and are proportional to the logarithm of the current density (Figure 2b and Figure 3b). Therefore, the incorporation rate of sulfur into nanoporous AAO films depends substantially on the applied voltage for each sulfuric acid concentration, and it is related to the electric field across the barrier layer. This fact is supported by the behavior of the variation of the barrier layer thickness with the electric field. As we mentioned before, the field-assisted flow increases for higher sulfuric acid concentration of the electrolyte for a given anodization voltage. This implies that the barrier layer is thinner for higher sulfuric acid concentrations for a given voltage. Following this statement and referring to our previous article, we can confirm this point since the interpore distance decreases for a given voltage as the sulfuric acid concentration increases.[49] Since the thickness of the barrier layer can be considered as half of the interpore

DOI: 10.1021/acs.jpcc.5b06928
J. Phys. Chem. C 2015, 119, 27392−27400

distance,[45] we can evaluate the barrier layer of our samples from the evolution of the interpore distances with the applied voltage. The barrier layer thickness decreases as the concentration of the sulfuric acid increases for a given applied voltage. Therefore, the current density increases, which implies that the volume expansion and the incorporation of sulfur atoms also increase.

3.5. Self-Ordering Degree. The dependence between the volume expansion factor and the self-ordering degree of the nanoporous AAO films is also studied (Figure 5). The self-ordering degree can be explained by means of mechanical stress due to the volume expansion.[46,47] Volume expansion causes mechanical stress at the metal/oxide interface as a consequence of repulsive forces.[45] Depending on the magnitude of the stress, it may lead to self-order or disorder, as well as macroscopic fractures across the alumina films. When the relation between applied voltage, current density, and acid concentration induces moderate volume expansion, stress is also moderate. Then, equilibrium exists among repulsive forces inducing self-ordering.[45] The plastic flow of the anodic alumina during the growth has been insightfully studied.[27,31] It is clear that the porous formation is associated with plastic deformation and flow of the oxide through the walls of the cells. Herbert et al. pointed out that self-ordering may be assisted by the stress distribution due to viscous flow of the oxide.[74] More recently, self-ordering has been attributed to the driving force of the asymmetrical distribution of the electric field.[55]

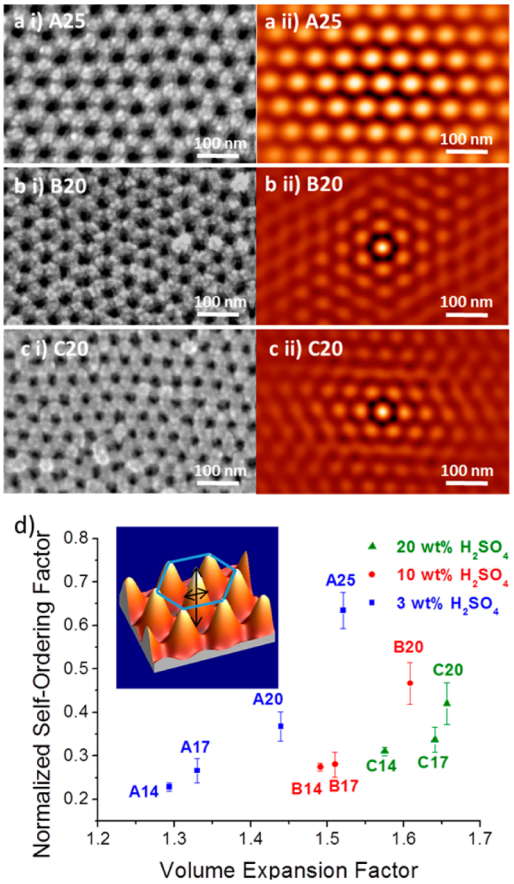

Figure 5. Top view of the SEM images (left) and their respective self-correlation images (right) for samples (a) A25, (b) B20, and (b) C20. (d) Normalized self-ordering factor of AAO nanopores as a function of the volume expansion factor (inset: 3D representation of the central spot of self-correlation image indicating the hexagonal pattern, amplitude, and full width at half-maximum).

In this case, the samples with the best self-ordering degree achieved is for samples A25 (Figure 5a), B20 (Figure 5b), and C20 (Figure 5c). The self-ordering of the nanopores is qualitatively evaluated by means of self-correlation images.[49] The images presented in Figure 5 [panels a–c (i)] correspond to small areas in order to help to visualize the qualitative evaluation of the self-ordering degree by means of self-correlation images [Figure 5, panels a–c (ii)]. For example, sample A25 (Figure 5a) shows a perfect hexagonal pattern; however, the whole sample is actually composed by different domains delimited by imperfections and defects on the hexagonal pattern. Self-correlation images from samples B20 (Figure 5b (ii) and C20 (Figure 5c (ii) also show hexagonal patterns, although slight defects in the hexagonal arrangement of the pores, as well as small defects on the surface, leads to lower quality on the hexagonal pattern of their respective self-correlation images. The quantitative evaluation of the self-ordering degree is represented in (Figure 5d). This evaluation has been carried out on images with approximately the same number of pores involving different domains in order to get a realistic normalized self-ordering factor.[49] The inset of Figure 5d shows the central spot of the self-correlation image. The amplitude of the maxima and full width at half-maximum for the central spot and the nearest neighbors are the parameters used for calculating the normalized self-ordering factor.[49] The samples with the best self-ordering factors have volume expansion factors ranging between 1.50 and 1.66 (Figure 5d). Other studies estimate that for self-ordering conditions the volume expansion factor should be between 1.2 and 1.4, independent of the electrolyte.[45−47] This difference could be explained taking into account that the calculations were carried out on the basis of stoichiometric alumina. However, especially in nanoporous AAO films grown in sulfuric acid based electrolytes, the incorporation of derived sulfur species from the electrolyte is very high,[26] therefore, the composition of the anodic alumina is different and the density of the nanoporous AAO is lower. This implies that the volume expansion factor for self-ordering should be higher. Figure 5d also shows that a determined volume expansion factor is not a decisive condition for achieving self-ordering in the nanoporous of nanoporous AAO films. For instance, maximum self-ordering is achieved for sample A25 with a value of the volume expansion factor of 1.51. Similar value of volume expansion factor is obtained for samples B14 and B17; however, their self-ordering degree is almost inexistent. These results agree with those presented by Ono et al.[61] That work shows that the optimal conditions for self-ordering are obtained at the highest electric fields possible while maintaining a uniform growth of alumina and avoiding the burning of the sample or electric breakdown. Therefore, the best self-ordering factors are obtained for the samples anodized at higher voltages under stable growth conditions. It is well-known that the mechanical stress is dependent on the formation rates.[75] The mechanical stress in samples B14 and B17 may not be high enough due to low formation rates of anodic alumina in comparison with A25 or B20 (Figure 5d). On the other hand, an increasing tendency of the self-ordering degree is observed in the B and C series as the volume expansion factor increases. We have observed a high self-ordering degree for samples B20 and C20 with volume expansion factors of 1.6 and 1.65, respectively. At this point, the plasticity of the nanoporous cells plays a key role in the self-

DOI: 10.1021/acs.jpcc.5b06928
J. Phys. Chem. C 2015, 119, 27392−27400

ordering arrangement. Plasticity in nanoporous AAO films can be defined as the tolerance or capacity of deformation under stress and adjustment among the cells of neighbor nanopores. The stress at the volume expansion factor of 1.6−1.65 is high, which may have led to disordered arrangement of nanopores. However, the sulfur incorporation is also high for samples B20 and C20 (Figure 5). The sulfur incorporation may enhance the plasticity of the nanoporous AAO films and facilitate the flow of the oxide toward the walls of the cells. Therefore, the formation of self-ordered nanopores under higher stress generated by the high volume expansion may be explained by an enhanced plasticity of the nanoporous AAO films. Our previous study shows that although there is a maximum self-ordering degree for each acid concentration that maximum is not the same for each one of them.[49] Therefore, it can be concluded that self-ordering regimes are not exclusively dependent on the volume expansion factor. However, there is a compromise between stress generated by volume expansion and plasticity of the nanoporous AAO film.

4. CONCLUSIONS

Three series of nanoporous AAO films are grown in sulfuric-based electrolytes at 3, 10, and 20 wt % concentration of sulfuric acid under potentiostatic conditions under 14−25 V. The analysis of RBS signal for these samples show an increase of the sulfur atoms incorporation within the nanoporous AAO films with the applied voltage and sulfuric acid concentration of the electrolyte. The S/Al ratio varies from 0.062 for the sample A14 up to 0.13 for sample C25. The values of volume expansion factor for the present anodic alumina films range between 1.29 and 1.66. On the one hand, there is a linear relation of sulfur incorporation and volume expansion with the applied voltage. On the other hand, there is a logarithmic dependence of sulfur atoms incorporation and the volume expansion factor on the average current density of the anodization processes (i.e, an exponential dependence of the current density on the incorporation of sulfur and the volume expansion), similar to the dependence on the applied voltage. These two facts suggest that both sulfur incorporation and volume expansion are governed by the electric field generated across the barrier layer. By the comparison of the results obtained in the present work with previous reports, we could conclude that the volume expansion factor evolution only depends on the current density, regardless if the nanoporous AAO films are grown under galvanostatic or potentiostatic conditions during a steady-state growth. Volume expansion and sulfur incorporation shows linear proportionality and depends on the concentration of the acid in the electrolyte. The slopes for each acid concentration in the electrolyte (3, 10, and 20 wt %) are 3.6, 5.7, and 12.3, respectively. Importantly, it has also been revealed that self-ordering conditions are obtained for high volume expansion factors. Moreover, the concentration of the electrolyte is another variable with which it is possible to look for improvement of self-ordering by optimizing the applied voltage during the anodization. High applied voltages with stable current densities and homogeneous growth avoiding burning or electrical breakdown also help to promote self-ordering. Sulfur incorporation increases the plastic flow of the oxide in the barrier layer and consequently the plasticity of the nanoporous AAO films under high stress values generated at high volume expansion factor values. The enhanced plasticity of the nanoporous AAO allows the formation of new self-ordering regimes at a high volume expansion factor. Therefore, we conclude that self-ordering conditions are obtained under balance of stress generated by volume expansion and the expected enhanced plasticity of the nanoporous AAO due to sulfur incorporation.

■ ASSOCIATED CONTENT

Supporting Information

The Supporting Information is available free of charge on the ACS Publications website at DOI: 10.1021/acs.jpcc.5b06928.

Average current density as a function of applied voltage; RBS spectra of S nuclei embedded in the nanoporous AAO films from the A, B, and C sample series anodized at 20, 17, and 14 V; growth rate as a function of applied voltage and current density; table with charge density and thickness of consumed aluminum and nanoporous AAO films after anodization (PDF)

■ AUTHOR INFORMATION

Corresponding Authors

*E-mail: denisfichou@ntu.edu.sg.

*E-mail: manuel.hernandez@uam.es.

Present Addresses

○School of Physical and Mathematical Science, Nanyang Technological University, 637371 Singapore.

□Instituto de cerámica y vidrio, Consejo Superior de Investigaciones Científicas, 28049 Cantoblanco, Madrid, Spain.

Author Contributions

The manuscript was written through contributions of all authors. All authors have given approval to the final version of the manuscript.

Notes

The authors declare no competing financial interest.

■ ACKNOWLEDGMENTS

Work supported by the Spanish Ministry of Science and Innovation under project MAT2010-20798-05-01 and 05-05. The authors wish to thank the support from the Ministry of Education in Singapore under the AcRF Tier 2 (MOE2014-T2-1-132). I.M.B. thanks the Spanish National Research Council (CSIC) for a JAE-preDoc fellowship cofinanced by the European Social Fund. M.H.-V. thanks financial support under project CCG08-UAM/MAT-4024.

■ REFERENCES

(1) Yuan, C.; Wu, H. B.; Xie, Y.; Lou, X. W. Mixed Transition-Metal Oxides: Design, Synthesis, and Energy-Related Applications. *Angew. Chem., Int. Ed.* **2014**, *53*, 1488−1504.

(2) Lang, X.; Hirata, A.; Fujita, T.; Chen, M. Nanoporous Metal/Oxide Hybrid Electrodes for Electrochemical Supercapacitors. *Nat. Nanotechnol.* **2011**, *6*, 232−236.

(3) Osterloh, F. E. Inorganic Nanostructures for Photoelectrochemical and Photocatalytic Water Splitting. *Chem. Soc. Rev.* **2013**, *42*, 2294−2320.

(4) Jakani, M.; Campet, G.; Claverie, J.; Fichou, D.; Pouliquen, J.; Kossanyi, J. Photoelectrochemical Properties of Zinc Oxide Doped with 3d Elements. *J. Solid State Chem.* **1985**, *56*, 269−77.

(5) Xia, X.; Zhang, Y.; Chao, D.; Guan, C.; Zhang, Y.; Li, L.; Ge, X.; Mínguez-Bacho, I.; Tu, J.; Fan, H. J. Solution Synthesis of Metal Oxides for Electrochemical Energy Storage Applications. *Nanoscale* **2014**, *6*, 5008−5048.

(6) Meyer, J.; Hamwi, S.; Kröger, M.; Kowalsky, W.; Riedl, T.; Kahn, A. Transition Metal Oxides for Organic Electronics: Energetics, Device Physics and Applications. *Adv. Mater.* **2012**, *24*, 5408−5427.

(7) Qi, H.; Wolfe, J.; Wang, D.; Fan, H. J.; Fichou, D.; Chen, Z. Triple-Layered Nanostructured Wo_3 Photoanodes with Enhanced Photocurrent Generation and Superior Stability for Photoelectrochemical Solar Energy Conversion. *Nanoscale* **2014**, *6*, 13457−13462.
(8) Minguez-Bacho, I.; Courté, M.; Fan, H. J.; Fichou, D. Conformal Cu_2s-Coated Cu_2o Nanostructures Grown by Ion Exchange Reaction and Their Photoelectrochemical Properties. *Nanotechnology* **2015**, *26*, 185401.
(9) Zhu, C.; Chao, D.; Sun, J.; Mínguez-Bacho, I.; Fan, Z.; Ng, C. F.; Xia, X. H.; Huang, H.; Zhang, H.; Shen, Z. X.; et al. Enhanced Lithium Storage Performance of Cuo Nanowires by Coating of Graphene Quantum Dots. *Adv. Mater. Interfaces* **2015**, *2*, 1400499.
(10) Hebert, K. R.; Albu, S. P.; Paramasivam, I.; Schmuki, P. Morphological Instability Leading to Formation of Porous Anodic Oxide Films. *Nat. Mater.* **2011**, *11*, 162−166.
(11) Ferre-Borrull, J.; Pallares, J.; Macias, G.; Marsal, L. F. Nanostructural Engineering of Nanoporous Anodic Alumina for Biosensing Applications. *Materials* **2014**, *7*, 5225−5253.
(12) Sola, L.; Alvarez, J.; Cretich, M.; Swann, M. J.; Chiari, M.; Hill, D. Characterization of Porous Alumina Membranes for Efficient, Real-Time, Flow through Biosensing. *J. Membr. Sci.* **2015**, *476*, 128−135.
(13) Kumeria, T.; Santos, A.; Rahman, M. M.; Ferre-Borrull, J.; Marsal, L. F.; Losic, D. Advanced Structural Engineering of Nanoporous Photonic Structures: Tailoring Nanopore Architecture to Enhance Sensing Properties. *ACS Photonics* **2014**, *1*, 1298−1306.
(14) Kumeria, T.; Santos, A.; Losic, D. Nanoporous Anodic Alumina Platforms: Engineered Surface Chemistry and Structure for Optical Sensing Applications. *Sensors* **2014**, *14*, 11878−11918.
(15) Caballero-Flores, R.; González-Legarreta, L.; Rosa, W. O.; Sánchez, T.; Prida, V. M.; Escoda, Ll.; Suñol, J. J.; Batdalov, A. B.; Aliev, A. M.; Koledov, V. V.; et al. Magnetocaloric Effect, Magnetostructural and Magnetic Phase Transformations in $Ni_{50.3}Mn_{36.5}Sn_{13.2}$ Heusler Alloy Ribbons. *J. Alloys Compd.* **2015**, *629*, 332−342.
(16) Bohnert, T.; Vega, V.; Michel, A. K.; Prida, V. M.; Nielsch, K. Magneto-Thermopower and Magnetoresistance of Single Co-Ni Alloy Nanowires. *Appl. Phys. Lett.* **2013**, *103*, 092407.
(17) Bran, C.; Palmero, E. M.; del Real, R. P.; Vazquez, M. CoFeCu Electroplated Nanowire Arrays: Role of Composition and Annealing on Structure and Magnetic Properties. *Phys. Status Solidi A* **2014**, *211*, 1076−1082.
(18) Palmero, E. M.; Bran, C.; del Real, R. P.; Magen, C.; Vazquez, M. Magnetic Behavior of NiCu Nanowire Arrays: Compositional, Geometry and Temperature Dependence. *J. Appl. Phys.* **2014**, *116*, 033908.
(19) Minguez-Bacho, I.; Rodriguez-Lopez, S.; Vazquez, M.; Hernandez-Velez, M.; Nielsch, K. Electrochemical Synthesis and Magnetic Characterization of Periodically Modulated Co Nanowires. *Nanotechnology* **2014**, *25*, 145301.
(20) Martín, J.; Martín-González, M.; Francisco Fernández, J.; Caballero-Calero, O. Ordered Three-Dimensional Interconnected Nanoarchitectures in Anodic Porous Alumina. *Nat. Commun.* **2014**, *5*, 5130.
(21) Lee, W.; Schwirn, K.; Steinhart, M.; Pippel, E.; Scholz, R.; Gosele, U. Structural Engineering of Nanoporous Anodic Aluminium Oxide by Pulse Anodization of Aluminium. *Nat. Nanotechnol.* **2008**, *3*, 234−239.
(22) Montero Moreno, J. M.; Waleczek, M.; Martens, S.; Zierold, R.; Gorlitz, D.; Martinez, V. V.; Prida, V. M.; Nielsch, K. Constrained Order in Nanoporous Alumina with High Aspect Ratio: Smart Combination of Interference Lithography and Hard Anodization. *Adv. Funct. Mater.* **2014**, *24*, 1857−1863.
(23) Keller, F.; Hunter, M. S.; Robinson, D. L. Structural Features of Oxide Coating on Aluminium. *J. Electrochem. Soc.* **1953**, *100*, 411−419.
(24) O'Sullivan, J. P.; Wood, G. C. Morphology and Mechanism of Formation of Porous Anodic Films on Aluminium. *Proc. R. Soc. London, Ser. A* **1970**, *317*, 511−543.
(25) Dekker, A.; Middelhoek, A. Transport Numbers and Structure of Porous Anodic Films on Aluminium. *J. Electrochem. Soc.* **1970**, *117*, 440−448.
(26) Thompson, G. E.; Wood, G. C. Porous Anodic Film Formation on Aluminium. *Nature* **1981**, *290*, 230−232.
(27) Oh, J.; Thompson, C. V. The Role of Electric Field in Pore Formation During Aluminum Anodization. *Electrochim. Acta* **2011**, *56*, 4044−4051.
(28) Wood, G. C.; Skeldon, P.; Thompson, G. E.; Shimizu, K. A Model for the Incorporation of Electrolyte Species into Anodic Alumina. *J. Electrochem. Soc.* **1996**, *143*, 74−83.
(29) Diggle, J.; Downie, T. C.; Goulding, C. W. Anodic Oxide Films on Aluminium. *Chem. Rev.* **1969**, *69*, 365.
(30) Garcia-Vergara, S. J.; Iglesias-Rubianes, L.; Blanco-Pinzon, C. E.; Skeldon, P.; Thompson, G. E.; Campestrini, P. Mechanical Instability and Pore Generation in Anodic Alumina. *Proc. R. Soc. London, Ser. A* **2006**, *462*, 2345−2358.
(31) Garcia-Vergara, S. J.; Skeldon, P.; Thompson, G. E.; Habazaki, H. A Flow Model of Porous Anodic Film Growth on Aluminium. *Electrochim. Acta* **2006**, *52*, 681−687.
(32) Garcia-Vergara, S. J.; Skeldon, P.; Thompson, G. E.; Habazaki, H. Stress Generated Porosity in Anodic Alumina Formed in Sulphuric Acid Electrolyte. *Corros. Sci.* **2007**, *49*, 3772−3782.
(33) Vrublevsky, I.; Parkoun, V.; Sokol, V.; Schreckenbach, J. Analysis of Chemical Dissolution of the Barrier Layer of Porous Oxide on Aluminum Thin Films Using a Re-Anodizing Technique. *Appl. Surf. Sci.* **2005**, *252*, 227−233.
(34) Han, H.; Park, S.-J.; Jang, J. S.; Ryu, H.; Kim, K. J.; Baik, S.; Lee, W. In Situ Determination of the Pore Opening Point During Wet-Chemical Etching of the Barrier Layer of Porous Anodic Aluminum Oxide: Nonuniform Impurity Distribution in Anodic Oxide. *ACS Appl. Mater. Interfaces* **2013**, *5*, 3441−3448.
(35) Ono, S.; Ichinose, H.; Masuko, N. The High-Resolution Observation of Porous Anodic Films Formed on Aluminium in Phosphoric-Acid Solution. *Corros. Sci.* **1992**, *33*, 841−850.
(36) Du, Y.; Cai, W. L.; Mo, C. M.; Chen, J.; Zhang, L. D.; Zhu, X. G. Preparation and Photoluminescence of Alumina Membranes with Ordered Pore Arrays. *Appl. Phys. Lett.* **1999**, *74*, 2951−2953.
(37) Vrublevsky, I.; Jagminas, A.; Hemeltjen, S.; Goedel, W. A. Effect of Heat Treatment on the Structure of Incorporated Oxalate Species and Photoluminescent Properties of Porous Alumina Films Formed in Oxalic Acid. *Appl. Surf. Sci.* **2008**, *254*, 7326−7330.
(38) Vojkuvka, L.; Santos, A.; Pallarès, J.; Ferré-Borrull, J.; Marsal, L. F.; Celis, J. P. On the Mechanical Properties of Nanoporous Anodized Alumina by Nanoindentation and Sliding Tests. *Surf. Coat. Technol.* **2012**, *206*, 2115−2124.
(39) Vrublevsky, I.; Parkoun, V.; Sokol, V.; Schreckenbach, J.; Marx, G. The Study of the Volume Expansion of Aluminum During Porous Oxide Formation at Galvanostatic Regime. *Appl. Surf. Sci.* **2004**, *222*, 215−225.
(40) Vrublevsky, I.; Parkoun, V.; Schreckenbach, J.; Marx, G. Effect of the Current Density on the Volume Expansion of the Deposited Thin Films of Aluminum during Porous Oxide Formation. *Appl. Surf. Sci.* **2003**, *220*, 51−59.
(41) Zhou, F.; Mohamed Al-Zenati, A. K.; Baron-Wiecheć, A.; Curioni, M.; Garcia-Vergara, S. J.; Habazaki, H.; Skeldon, P.; Thompson, G. E. Volume Expansion Factor and Growth Efficiency of Anodic Alumina Formed in Sulphuric Acid. *J. Electrochem. Soc.* **2011**, *158*, C202−C214.
(42) Kao, T. T.; Chang, Y. C. Influence of Anodization Parameters on the Volume Expansion of Anodic Aluminum Oxide Formed in Mixed Solution of Phosphoric and Oxalic Acids. *Appl. Surf. Sci.* **2014**, *288*, 654−659.
(43) Zhou, F.; Baron-Wiecheć, A.; Garcia-Vergara, S. J.; Curioni, M.; Habazaki, H.; Skeldon, P.; Thompson, G. E. Effects of Current Density and Electrolyte Temperature on the Volume Expansion Factor of Anodic Alumina Formed in Oxalic Acid. *Electrochim. Acta* **2012**, *59*, 186−195.

DOI: 10.1021/acs.jpcc.5b06928
J. Phys. Chem. C 2015, 119, 27392−27400

(44) Abd-Elnaiem, A. M.; Mebed, A. M.; Gaber, A.; Abdel-Rahim, M. A. Effect of the Anodization Parameters on the Volume Expansion of Anodized Aluminum Films. *Int. J. Electrochem. Sci.* **2013**, *8*, 10515−10525.
(45) Nielsch, K.; Choi, J.; Schwirn, K.; Wehrspohn, R. B.; Gosele, U. Self-Ordering Regimes of Porous Alumina: The 10% Porosity Rule. *Nano Lett.* **2002**, *2*, 677−680.
(46) Li, A. P.; Muller, F.; Birner, A.; Nielsch, K.; Gosele, U. Hexagonal Pore Arrays with a 50−420 nm Interpore Distance Formed by Self-Organization in Anodic Alumina. *J. Appl. Phys.* **1998**, *84*, 6023−6026.
(47) Jessensky, O.; Muller, F.; Gosele, U. Self-Organized Formation of Hexagonal Pore Arrays in Anodic Alumina. *Appl. Phys. Lett.* **1998**, *72*, 1173−1175.
(48) Hillebrand, R.; Muller, F.; Schwirn, K.; Lee, W.; Steinhart, M. Quantitative Analysis of the Gram Morphology in Self-Assembled Hexagonal Lattices. *ACS Nano* **2008**, *2*, 913−920.
(49) Mínguez-Bacho, I.; Rodríguez-López, S.; Asenjo, A.; Vázquez, M.; Hernández-Vélez, M. Self-Correlation Function for Determination of Geometrical Parameters in Nanoporous Anodic Alumina Films. *Appl. Phys. A: Mater. Sci. Process.* **2012**, *106*, 105−112.
(50) Romero, V.; Vega, V.; Garcia, J.; Zierold, R.; Nielsch, K.; Prida, V. M.; Hernando, B.; Benavente, J. Changes in Morphology and Ionic Transport Induced by Ald Sio2 Coating of Nanoporous Alumina Membranes. *ACS Appl. Mater. Interfaces* **2013**, *5*, 3556−3564.
(51) Zaraska, L.; Stepniowski, W. J.; Sulka, G. D.; Ciepiela, E.; Jaskula, M. Analysis of Nanopore Arrangement and Structural Features of Anodic Alumina Layers Formed by Two-Step Anodizing in Oxalic Acid Using the Dedicated Executable Software. *Appl. Phys. A: Mater. Sci. Process.* **2014**, *114*, 571−577.
(52) Pourfard, M.; Faez, K.; Tabaian, S. H. Autocorrelation-Based Method for Characterization of the Self-Hexagonal Lattice. *J. Phys. Chem. C* **2013**, *117*, 17225−17236.
(53) Borba, J. R.; Brito, C.; Migowski, P.; Vale, T. B.; Stariolo, D. A.; Teixeira, S. R.; Feil, A. F. Quantitative Characterization of Hexagonal Packings in Nanoporous Alumina Arrays: A Case Study. *J. Phys. Chem. C* **2013**, *117*, 246−251.
(54) Zaraska, L.; Stępniowski, W. J.; Ciepiela, E.; Sulka, G. D. The Effect of Anodizing Temperature on Structural Features and Hexagonal Arrangement of Nanopores in Alumina Synthesized by Two-Step Anodizing in Oxalic Acid. *Thin Solid Films* **2013**, *534*, 155−161.
(55) Kim, M.; Kim, H.; Bae, C.; Lee, J.; Yoo, H.; Moreno, J. M. M.; Shin, H. Initial Self-Ordering of Porous Anodic Alumina: Transition from Polydispersity to Monodispersity. *J. Phys. Chem. C* **2014**, *118*, 26789−26795.
(56) Masuda, H.; Hasegwa, F.; Ono, S. Self-Ordering of Cell Arrangement of Anodic Porous Alumina Formed in Sulfuric Acid Solution. *J. Electrochem. Soc.* **1997**, *144*, L127−L130.
(57) Masuda, H.; Satoh, M. Fabrication of Gold Nanodot Array Using Anodic Porous Alumina as an Evaporation Mask. *Jpn. J. Appl. Phys.* **1996**, *35*, L126−L129.
(58) Climent-Font, A.; Paszti, F.; Garcia, G.; Fernandez-Jimenez, M. T.; Agullo, F. First Measurements with the Madrid 5 Mv Tandem Accelerator. *Nucl. Instrum. Methods Phys. Res., Sect. B* **2004**, *219-220*, 400−404.
(59) Mayer, M. Simnra, a Simulation Program for the Analysis of NRA, RBS and ERDA. In *Aip. Conf. Proc.*, Duggan, J. L., Morgan, I. L., Eds.; AIP: College Park, MD, 1998; Vol. *475*, pp 541−544.10.1063/1.59188
(60) Houser, J. E.; Hebert, K. R. Stress-Driven Transport in Ordered Porous Anodic Films. *Phys. Status Solidi A* **2008**, *205*, 2396−2399.
(61) Ono, S.; Saito, M.; Ishiguro, M.; Asoh, H. Controlling Factor of Self-Ordering of Anodic Porous Alumina. *J. Electrochem. Soc.* **2004**, *151*, B473−B478.
(62) Sulka, G. D.; Stroobants, S.; Moshchalkov, V.; Borghs, G.; Celis, J. P. Synthesis of Well-Ordered Nanopores by Anodizing Aluminum Foils in Sulfuric Acid. *J. Electrochem. Soc.* **2002**, *149*, D97−D103.
(63) Thompson, G. E.; Furneaux, R. C.; Wood, G. C.; Richardson, J. A.; Goode, J. S. Nucleation and Growth of Porous Anodic Films on Aluminium. *Nature* **1978**, *272*, 433−435.
(64) Patermarakis, G.; Moussoutzanis, K.; Nikolopoulos, N. Investigation of the Incorporation of Electrolyte Anions in Porous Anodic Al2o3 Films by Employing a Suitable Probe Catalytic Reaction. *J. Solid State Electrochem.* **1999**, *3*, 193−204.
(65) Patermarakis, G.; Chandrinos, J.; Moussoutzanis, K. Interface Physicochemical Processes Controlling Sulphate Anion Incorporation in Porous Anodic Alumina and Their Dependence on the Thermodynamic and Transport Properties of Cations. *J. Electroanal. Chem.* **2001**, *510*, 59−66.
(66) Ono, S.; Masuko, N. The Duplex Structure of Cell-Walls of Porous Anodic Films Formed on Aluminium. *Corros. Sci.* **1992**, *33*, 503−507.
(67) Thompson, G. E. Porous Anodic Alumina: Fabrication, Characterization and Applications. *Thin Solid Films* **1997**, *297*, 192−201.
(68) Michalska-Domanska, M.; Norek, M.; Stępniowski, W. J.; Budner, B. Fabrication of High Quality Anodic Aluminum Oxide (AAO) on Low Purity Aluminum-a Comparative Study with the Aao Produced on High Purity Aluminum. *Electrochim. Acta* **2013**, *105*, 424−432.
(69) Stępniowski, W. J.; Bojar, Z. Synthesis of Anodic Aluminum Oxide (Aao) at Relatively High Temperatures. Study of the Influence of Anodization Conditions on the Alumina Structural Features. *Surf. Coat. Technol.* **2011**, *206*, 265−272.
(70) Almasi Kashi, M.; Ramazani, A. The Effect of Temperature and Concentration on the Self-Organized Pore Formation in Anodic Alumina. *J. Phys. D: Appl. Phys.* **2005**, *38*, 2396−2399.
(71) Sulka, G. D.; Parkola, K. G. Temperature Influence on Well-Ordered Nanopore Structures Grown by Anodization of Aluminium in Sulphuric Acid. *Electrochim. Acta* **2007**, *52*, 1880−1888.
(72) Li, F. Y.; Zhang, L.; Metzger, R. M. On the Growth of Highly Ordered Pores in Anodized Aluminum Oxide. *Chem. Mater.* **1998**, *10*, 2470−2480.
(73) Verwey, E. J. W. Electrolytic Conduction of a Solid Insulator at High Fields - the Formation of the Anodic Oxide Film on Aluminium. *Physica* **1935**, *2*, 1059−1063.
(74) Houser, J. E.; Hebert, K. R. The Role of Viscous Flow of Oxide in the Growth of Self-Ordered Porous Anodic Alumina Films. *Nat. Mater.* **2009**, *8*, 415−420.
(75) Bradhurst, D. H.; Llewelyn Leach, J. S. The Mechanical Properties of Thin Anodic Films on Aluminum. *J. Electrochem. Soc.* **1966**, *113*, 1245−1249.

DOI: 10.1021/acs.jpcc.5b06928
J. Phys. Chem. C 2015, 119, 27392−27400